Received: 29 December 2024 | Revised: 16 January 2025 | Accepted: 18 January 2025

DOI: 10.1002/pen.27118

RESEARCH ARTICLE

POLYMER ENGINEERING AND SCIENCE WILEY

Effect of blown air temperature on morphology, phase structure and filtration efficiency of PVDF nanofibrous mats produced via electro-blowing

Ali Toptaş[1] | **Mehmet Durmuş Çalışır**[1,2] | **Mehmet Ali Tibatan**[1,3]

[1]TEMAG Labs, Faculty of Textile Technologies and Design, Istanbul Technical University, Istanbul, Turkey

[2]Faculty of Engineering and Architecture, Recep Tayyip Erdogan University, Rize, Turkey

[3]Faculty of Engineering and Natural Science, Istanbul Sabahattin Zaim University, Istanbul, Turkey

Correspondence
Ali Toptaş, TEMAG Labs, Faculty of Textile Technologies and Design, Istanbul Technical University, Istanbul, Turkey.
Email: atoptas34@gmail.com

Abstract

This study investigates the effects of temperature of pressurized blown air on fiber morphology, porosity, phase structure, and filtration performance of PVDF nanofibers produced via the electro-blowing method for the first time. The blown air heated to 20, 40, 60, and 80°C was utilized during production. Increasing air temperature resulted in more homogeneous distribution of fibers and defect-free fibrous mats, accompanied by a significant reduction in fiber diameter. A linear relationship between fiber diameter and pore size was observed; as fiber diameter decreased, reducing air permeability due to smaller pore sizes. FTIR measurements revealed the highest β-phase content (82%) in the PVDF-80C sample produced at 80°C. The rise in temperature lowered solution viscosity and surface tension, contributing to improved drawing effect and therefore higher β-phase content in the PVDF polymer. Corona discharge treatment further enhanced the surface potential, with the finest fibers exhibiting the highest surface charge. The PVDF-80C sample demonstrated the best performance during filtration tests against NaCl aerosols ($PM_{0.3}$) at a flow rate of 95 L/min, achieving a filtration efficiency of 98.68% with a pressure drop of 153 Pa. These findings highlight the critical role of temperature in influencing nanofiber properties and filtration performance.

Highlights

- Finer fibers and defect-free mats achieved with increased air temperature.
- PVDF-80C showed 82% β-phase content, the highest among all samples.
- Smaller fiber diameter led to reduced pore size and lower air permeability.
- Corona discharge enhanced surface potential, boosting fiber charge.
- PVDF-80C achieved 98.68% filtration efficiency *with* 153 Pa pressure drop.

KEYWORDS

air filter, crystallization, electro-blowing, PVDF, temperature

1 | INTRODUCTION

Air pollution has become a global public health concern due to anthropogenic activities such as industrialization, urbanization, and the combustion of fossil fuels[1,2] and maintaining air quality is critical for ensuring a sustainable future.[3] Particulate matter (PM), a major component of air pollution, enters the body through inhalation and has been linked to respiratory and cardiovascular diseases, oxidative stress, and inflammation.[4–6] Prolonged exposure to PM has been associated with severe health issues and premature mortality.[7,8] *PM is classified based on aerodynamic diameter, with PM_{10} and $PM_{2.5}$ referring to particles <10 and 2.5 μm, respectively. $PM_{0.3}$, with a diameter of 0.3 μm, is particularly critical as it represents the most penetrating particle size through filters and poses higher health risks by reaching the alveolar region of the lungs.*[9]

Consequently, effective filtration solutions to mitigate PM exposure are essential and play vital role in improving air quality by capturing particulate matter.[10] Among filtration materials and methods, nanofibrous fabrics, and mechanisms such as interception, diffusion, and electrostatic attraction stand out as effective approaches. Notably, electret nanofibrous structures have gained attention for their exceptional particle capture efficiency, attributed to their large surface area and small pore size, making them suitable for both indoor and outdoor air filtration applications.[11,12]

The filtration performance of nanofibrous mats depends on factors such as fiber diameter, surface area, and pore structure, all of which are influenced by production methods.[13,14] Techniques such as electrospinning (ES), solution blowing (SB), and centrifugal spinning (CS) enable the fabrication of nanofibers with diverse dimensions and properties.[15] Recently, the electro-blowing method (EB), which combines ES and SB techniques, has emerged as an innovative approach.[16] EB method offers significant advantages over SB and ES, including more homogeneous fiber distribution, finer fiber diameters, higher production rates, and improved industrial adaptability.[17–20]

Electret filters, with their ability to retain electrostatic charges, effectively capture particulate matter through filter media, thereby significantly enhancing air quality.[21,22] These filters provide high filtration efficiency, low pressure drop, energy savings, and sustained performance over extended use.[23] Polyvinylidene fluoride (PVDF), a material frequently used in electret filters, stands out due to its high dielectric constant and piezoelectric properties.[24] The β-phase of PVDF enhances its electrostatic charge retention capacity, thereby improving filtration efficiency.[25] Factors influencing the β-phase formation in PVDF include the applied electric field (poling), drawing rate, and process parameters.[26] Optimizing these parameters promotes β-phase transition in PVDF, maximizing its piezoelectric properties and enabling the production of higher-performance electret filters, thereby contributing to more effective solutions for air pollution mitigation.[27] Among the process parameters, relative humidity (RH) and environmental temperature play a critical role in determining the surface morphology and β-phase content ($\%F(\beta)$) of PVDF nanofibers. RH influences the evaporation rate of the solvent by forming a water layer on the PVDF jet surface, which slows solvent evaporation. This process provides more time for β-phase crystallization, facilitating the rearrangement of molecular chains.[28] For example, Zaarour et al. demonstrated that increasing RH from 2% to 62% resulted in an increase in $\%F(\beta)$ from 55% to 73.06%, accompanied by a transformation of nanofiber surfaces from smooth to wrinkled.[29] However, excessive RH can hinder solvent evaporation entirely, complicating the ES process.[30] The temperature also affects solvent volatilization rates and decreases solution surface tension and viscosity. These changes generate higher elongation forces on the jet, reducing nanofiber diameter and increasing $\%F(\beta)$.[27] Huang et al. reported that raising the temperature from 5°C to 45°C reduced the solution's surface tension from 41.23 to 27.05 mN/m and viscosity from 241.8 to 112.6 cP, thereby enhancing $\%F(\beta)$.[31] However, excessively high temperatures (>90°C) may inhibit β-phase formation, as the stable phase at elevated temperatures is the α-phase.[32]

This study, for the first time, investigates the effects of pressurized air heated to different temperatures in the EB technique on the morphology of fibers and fibrous mats, PVDF crystallization, and filtration performance. SEM analyses revealed that increasing the air temperature led to finer fibers and more uniform, defect-free mats. Elevated temperatures promoted β-phase formation, allowing the fibers to achieve higher surface potential values both immediately after production and following corona discharge treatment. Filtration performance and quality factors demonstrated a positive linear relationship with increasing air temperature.

2 | EXPERIMENTAL

2.1 | Materials

PVDF powder, with a molecular weight of 477,000 g/mol, was sourced from *Arkema Chemicals, France* (*Kynar Flex 2801-00*). Dimethyl sulfoxide (*DMSO, 99.8% purity, Merck, Germany*) and acetone (*99.5% purity, ISOlab, Germany*) served as the solvents. To prepare a 12 wt.% PVDF solution, the polymer was dissolved in a solvent mixture of acetone and DMSO at a weight ratio of 30:70. The solution was stirred magnetically at 70°C for 8 h. *The viscosity of the solution was measured as 453.2 mPa.s at room temperature (∼20°C).*

2.2 | Methods

2.2.1 | Production of nanofibrous mats

Nanofibrous webs were produced using a commercial EB system (Aerospinner, Areka Ltd., *Türkiye*). As depicted in Figure 1, the EB system comprised a compressed air tank connected to a regulator, a high-voltage power source, a syringe pump, a co-axial spinning nozzle mounted on a *homogenizer unit* to ensure uniform fiber deposition, and a vacuum-assisted rotating collector with a surface area of 38 × 33 cm^2. The production process involved a feeding rate of 10 ml/h, an air pressure of 1 bar, and an electric field strength of 30 kV, with a 30 cm gap between the nozzle and the collector. *The blown air is supplied from a compressed air tank and regulated using a pressure regulator. Before reaching the nozzle tip to blow the polymer solution into fibers, the air is heated by an electrical heating unit. The blown air temperature is measured at the nozzle tip using a contactless temperature-measuring device (UT306S, UNI-T, China). To achieve blown air temperatures of 40°C, 60°C, and 80°C at the nozzle tip, the air heater may need to heat the air to slightly higher temperatures than the measured value. Once the desired temperature was reached at the nozzle tip, feeding was initiated using a syringe pump, and production commenced. During production, the temperature was periodically measured and monitored to ensure it remained at the desired level. Additionally, sample codes were designated based on the nozzle tip temperature during the blowing process. For instance, samples produced at room temperature were simply labeled as PVDF, while PVDF-40C denoted samples produced with a nozzle tip temperature of 40°C.* The nanofibrous mats were collected over 1 h on a 20 gsm polypropylene (PP) spunbond nonwoven substrate.

2.2.2 | Morphology and fiber diameter of the samples

SEM images of the web samples were captured using the Tescan Vega 3 microscope to perform qualitative characterization of the webs. Additionally, the ImageJ software was utilized to measure the average fiber diameter (*AFD*) for both preliminary and main samples. The images were acquired at magnifications of 2 and 10 kX. Before SEM imaging, the samples were coated with a gold–palladium (AuPd) layer using a fine coater to prepare them for investigation.

2.2.3 | Corana charging and surface potential analysis

Corona charging was performed using a negative corona discharge device (Chargemaster 5, Simco Ion). During the process, the device's electrode was positioned roughly 4 cm above a rotating drum. The nanofibrous mats were mounted on the drum, which rotated at a speed of 23 rpm, and were charged for 5 min under a voltage of −20 kV.

The surface potential of the samples after corona charging was determined using a electrostatic Fieldmeter (FMX-004, SIMCO, Japan). Measurements were recorded from different regions of the samples, and the average surface potential was calculated.

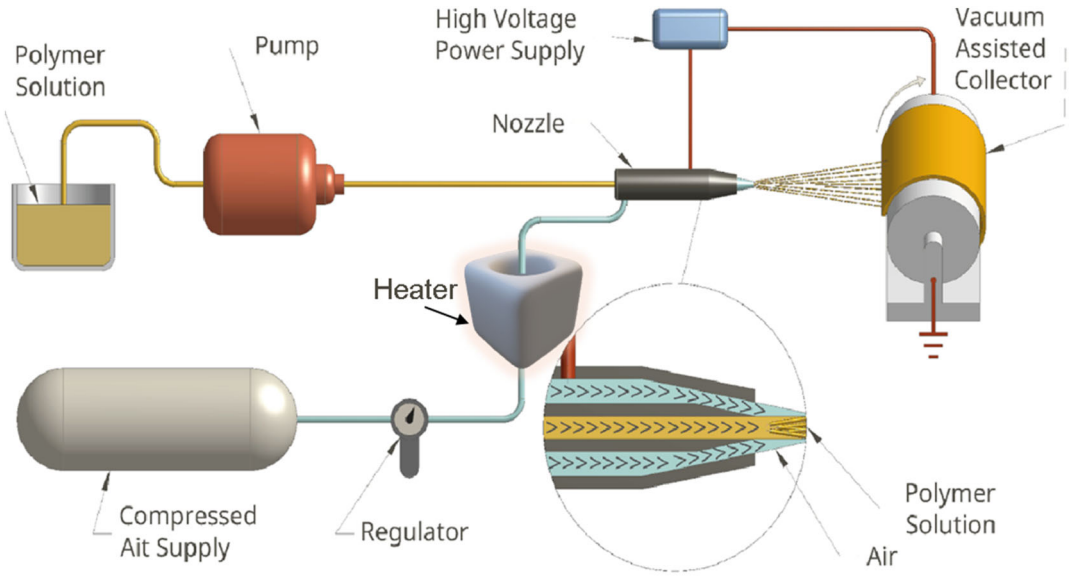

FIGURE 1 Schematic presentation of the EB device (adapted from Toptaş et al.[33]).

2.2.4 | Filtration performance test

To assess the filtration performance of the samples, an automatic filter testing machine (*8130A, TSI Inc., USA*) was used to measure pressure drop (ΔP) and filtration efficiency (η). Solid salt particles with an average diameter of $0.26 \pm 0.07\,\mu m$ were produced from a 2% by weight NaCl solution. Nanofibrous mats with an effective surface area of $100\,cm^2$ were tested against NaCl aerosols at a face velocity of 15.83 cm/s (corresponding to an air flow rate of 95 L/min). η was calculated using Equation (1).

$$\eta = 1 - C_{down}/C_{up} \tag{1}$$

where C_{down} and C_{up} represent the downstream and upstream particle concentration, respectively. The quality factor (QF), which assesses the filter sample's performance by accounting for both η and ΔP, is expressed mathematically in Equation (2).

$$QF = -\frac{ln(1-\eta)}{\Delta P} \tag{2}$$

3 | RESULTS AND DISCUSSIONS

The SEM images and fiber diameter distributions of the produced samples are presented in Figure 2. The fibrous network structures observed in all samples indicate successful fabrication. All samples exhibited fibers with a round morphology, and bundle formations (indicated by arrows) were observed. In the low-magnification SEM images shown in Figure 2a1–d1, the density and size of droplets (highlighted with dashed circles) decreased as the air temperature increased. Additionally, increasing air temperature resulted in a reduction in fiber diameters and a narrowing of diameter distributions. The *AFD* decreased from 172.0 ± 77.6 nm at *20°C blown air* to 165.1 ± 46.0, 149.8 ± 59.9, and 140.9 ± 55.7 nm as the temperature increased *from 40°C to 60°C and 80°C, respectively*. This reduction in fiber diameters and the decrease in defects within the mats can be attributed to the decreased solution viscosity and increased solvent evaporation rate at higher temperatures. *Additionally, the solution inside the needle is exposed to hot air at temperatures higher than those measured at the tip of the nozzle before it reaches the nozzle tip and is blown into nanofibers*. Lower solution viscosity facilitated the formation of finer fibers, while the higher solvent evaporation rate reduced the size and number of droplets. Furthermore, as shown in Figure 2a2–d2 (indicated by arrows), the decrease in fiber diameters also led to the formation of finer fiber bundles.

The effect of blown air temperature on the morphology of nanofibrous mats is schematically illustrated in Figure 3. With increasing the temperature, the rheological properties of the solution change, leading to a reduction in the size of the solution meniscus at the nozzle tip and a thinning of the wet polymer jets. As a result, less dense droplet formations and thinner fibers are collected on the collector, forming fibril mats with finer morphologies. While the increase in temperature of blown air does not have a direct effect on whether the fibers are formed in a single or bundled format, the reduction in fiber diameter leads to a corresponding decrease in bundle diameters. Additionally, the faster drying of the wet polymer jet at higher temperatures, coupled with the increased stretching of the fibers along the nozzle-to-collector distance, is believed to contribute to a higher β-phase content in the resulting nanofibers.

PVDF commonly exhibits α, β, and γ phases, depending on the molecular chain conformation during the production process. Among these phases, the β-phase features a structure where the electronegative fluorine groups and electropositive hydrogen groups are aligned alternately along the polymer chain. This phase exhibits the highest piezoelectric activity, which significantly enhances the electret properties of PVDF, making it advantageous for various applications, including its use as an air filter.[34] According to the detailed FTIR analysis conducted by Cai et al.[35] on PVDF, the characteristic bands for the α-phase are identified at 410, 489, 532, 614, 763, 795, 854, 975, 1149, 1209, 1383, and 1423 cm^{-1}; for the β-phase at 445, 473, and 1275 cm^{-1}; and for the γ-phase at 431, 482, 811, and 1234 cm^{-1}.

Based on the FTIR spectra in Figure 4A, all samples exhibit peaks at similar bands. The intense peaks observed at 1430, 1276, 840, and 510 cm^{-1}, along with the weak peaks at 614 and 760 cm^{-1}, indicate that the structures predominantly contain the β-phase with a minor presence of the α phase. The absence of peaks at 1234 and 811 cm^{-1}, which are characteristic of the γ phase, confirms that the γ-phase is not present in the samples. Furthermore, as air temperature increases, the resulting thinner fibers provide a larger surface area. This leads to more pronounced peaks in the FTIR spectra, as clearly shown in Figure 4B. The finer fibers likely enhance dipole interactions, enabling more efficient light absorption, as suggested by the more intense peaks observed.

The proportion of β-phase in each sample can be calculated using the approach outlined by Gregario and Cestari.[32] Based on the assumption that the IR absorption spectra adhere to Beer–Lambert's law, the absorbances at 840 cm^{-1} (A_β) and 760 cm^{-1} (A_α) are used, as specified in Equations (3) and (4).

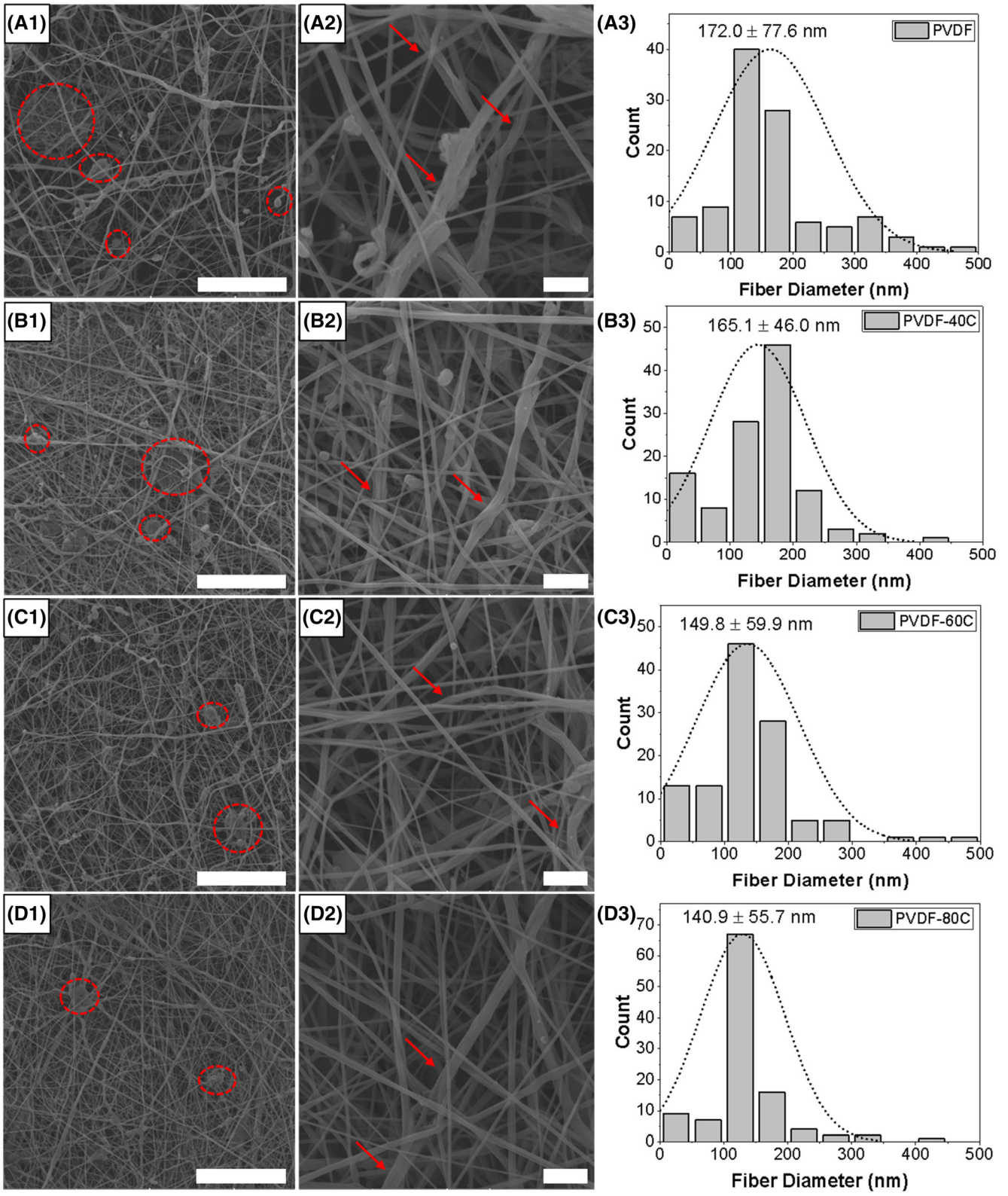

FIGURE 2 SEM images and fiber diameter distributions for (A) PVDF, (B) PVDF-40C, (C) PVDF-60C, and (D) PVDF-80C samples (scale bars are 5 and 2 μm for column 1 and 2, respectively).

$$A_{\propto} = log\frac{I_{\propto}^{0}}{I_{\propto}} \quad (3)$$

$$A_{\beta} = log\frac{I_{\beta}^{0}}{I_{\beta}} \quad (4)$$

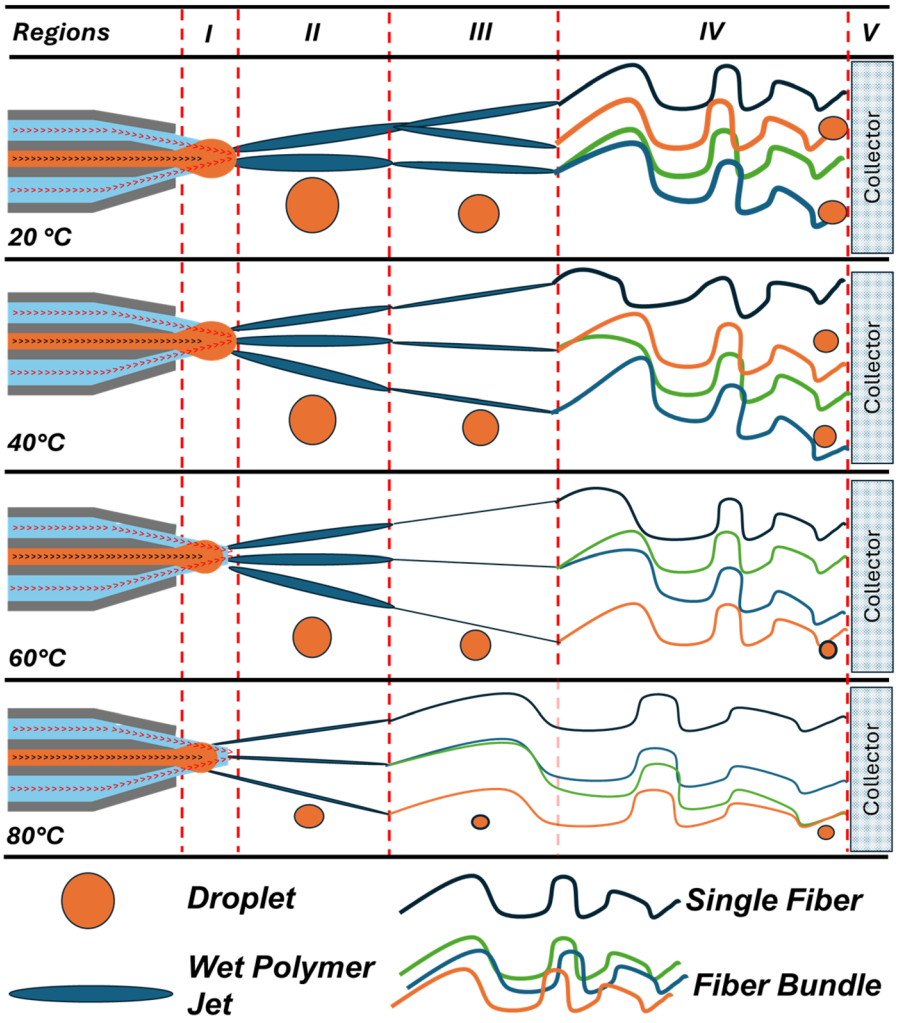

FIGURE 3 Illustration of the effects of blown air temperature on the polymer jet and the resulting arrangement of nanofibrous mats.

$$F(\beta) = \frac{X_\beta}{X_\alpha + X_\beta} = \frac{A_\beta}{1.3A_\alpha + A_\beta} \quad (5)$$

Here, I and I^o represent the intensities of the transmitted and incident radiation, respectively. For a system containing both β-phase and α-phase, the relative fraction of the β-phase, $F(\beta)$, can be calculated using Equation (5).[32] Based on these calculations, the PVDF, PVDF-40, PVDF-60, and *PVDF-80C* samples contain 76%, 77%, 76%, and 82% β-phase, respectively. The presence of an electric field during all production processes facilitated the formation of the β-phase, consistently achieving levels above 76%. Furthermore, higher air temperatures led to faster solvent evaporation, increased mechanical stretching and the formation of finer fibers, resulting in the maximum β-phase content in the *PVDF-80C* sample.

Air permeability is defined as "the amount of airflow passing perpendicularly through a material between its two surfaces under a specific differential air pressure.".[36] It is a critical factor in evaluating the performance of filter fabrics and is directly related to the thickness and pore structure of the samples. The air permeability results of the samples are presented in Figure 5A. As the temperature of the pressurized air increased during production (from PVDF to *PVDF-80C*), the air permeability decreased from 44.9 to 32.5 cfm. Since the amount of fiber and thickness of the fibrous mats was considered the same, this was only associated with the AFDs in the mats, as shown in Figure 5B. As the fiber diameters decreased, the pores in the mats became narrower, resulting in lower air permeability values.

The η values of PVDF samples against NaCl aerosol particles with a size of 0.26 ± 0.07 µm are presented in Figure 6. The effect of the nanofibrous structure was observed in all samples, with the η measured at a minimum of 84.23%, even in the lowest-performing sample. The decrease in fiber diameter due to the increase in pressurized air temperature during production led to improved the η. The PVDF-80C sample, which featured the thinnest fibers, exhibited an η of 93.81%, making it

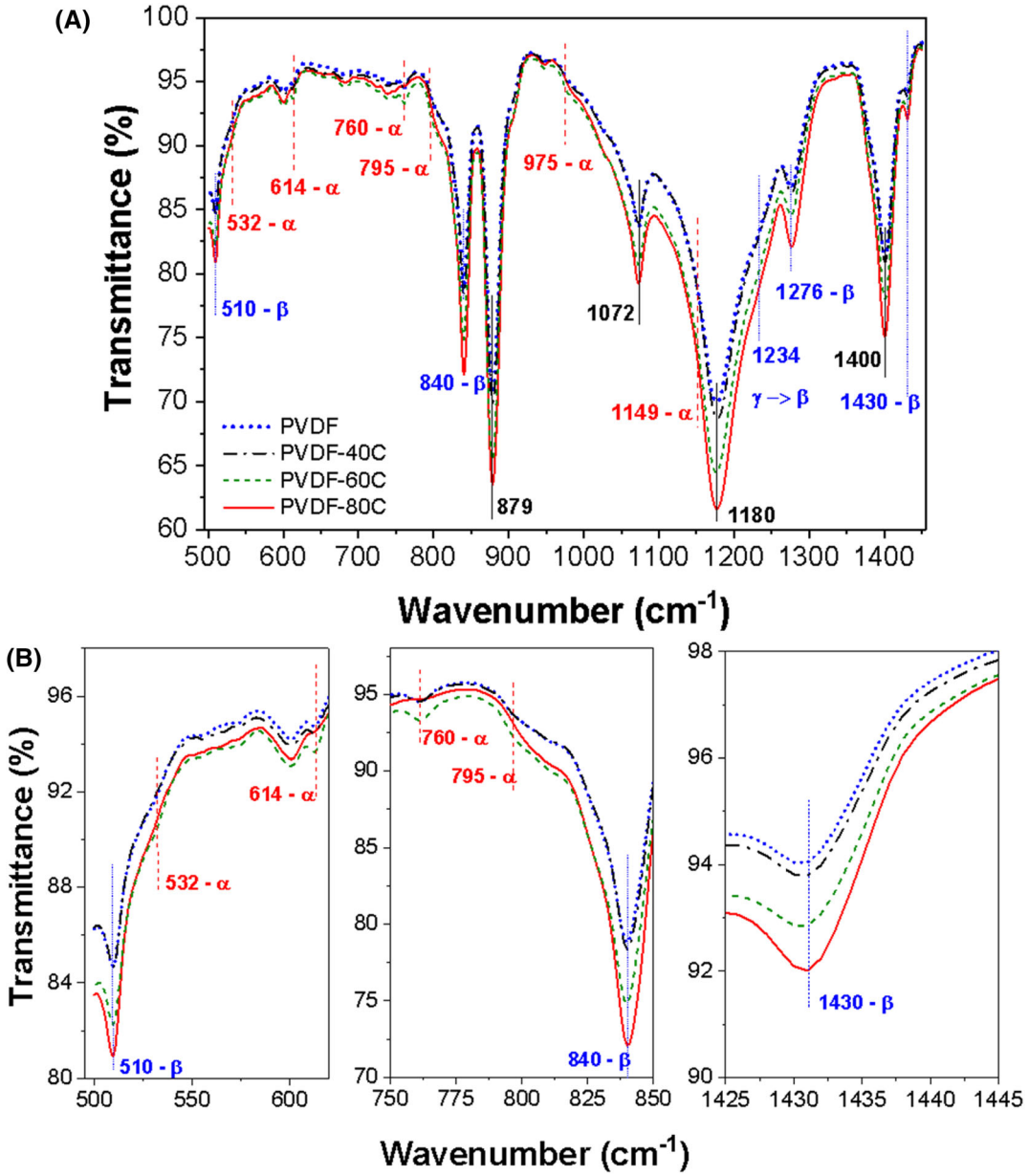

FIGURE 4 (A) FTIR spectrum of the samples in the range of 500–1450 cm^{-1} and (B) its enlarged version highlighting specific regions for detailed analysis.

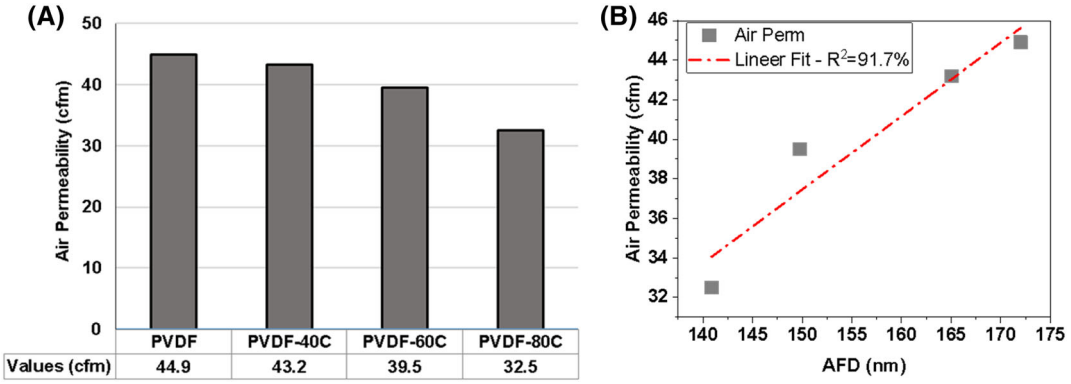

FIGURE 5 (A) Air permeability of the samples and (B) relationship between air permeability and AFDs.

the best-performing sample. As shown in Figure 5B, the corona discharge process resulted in a significant increase in the η across all samples, without causing a notable rise in pressure drop. The PVDF sample, which showed the lowest η before treatment, achieved 89.91% after corona charging. The highest η was observed in the PVDF-80C sample, with an η of 98.68% at a ΔP of 153 Pa.

In Figure 7, the QF values of the samples before and after corona discharge treatment are analyzed. Since the ΔP values remained nearly constant, the observed improvement in QF values can be attributed to increased efficiency. Prior to the corona discharge treatment, the QF values were found to increase as the fiber diameters decreased. Similarly, after the corona discharge treatment, the QF values improved for all fibers, with the degree of improvement being directly proportional to the reduction in fiber diameter. The PVDF-80C sample exhibited the highest improvement, with a 48% increase in QF. Figure 7B illustrates the relative percentage changes in AFDs and surface potential improvements for the PVDF sample. The increase in air temperature led to fibers that were approximately 5% to 20% thinner. This reduction in fiber diameter contributed to the improvement in QFs, as thinner fibers retained more electric charges, resulting in higher surface potentials. This effect manifests itself in the surface potential values of the fibers both before and after corona discharge treatment as shown in Table 1. Furthermore, the greater β-phase content in this sample enhanced its electret properties, enabling better surface charge retention and contributing to its superior performance.

Figure 8 illustrates the relationship between temperature of blown air and filtration performance, surface potential, and the *AFD* of the produced samples. The results

TABLE 1 Surface potential of the samples before and after corona discharge treatment.

	Surface potential (kV)	
Samples	**Before**	**After**
PVDF	−0.43	−0.63
PVDF-40C	−0.52	−0.69
PVDF-60C	−0.58	−0.73
PVDF-80C	−0.6	−0.74

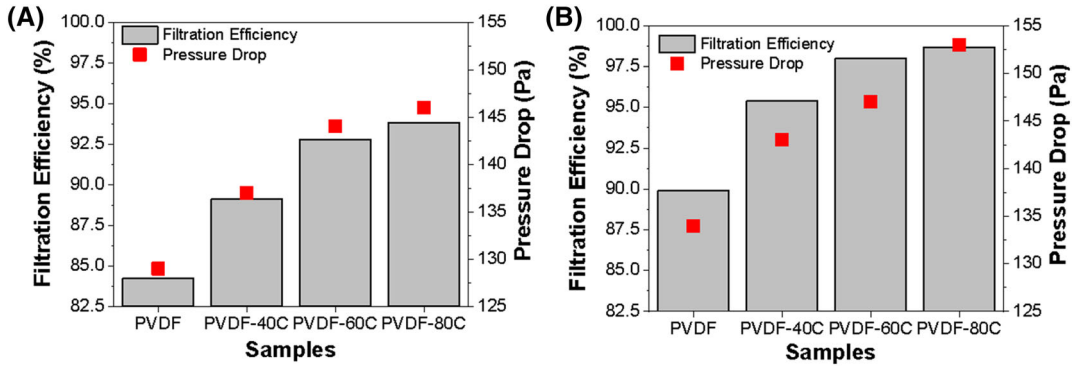

FIGURE 6 Filtration efficiency and pressure drop values of the samples (A) before and (B) after corona discharge treatment.

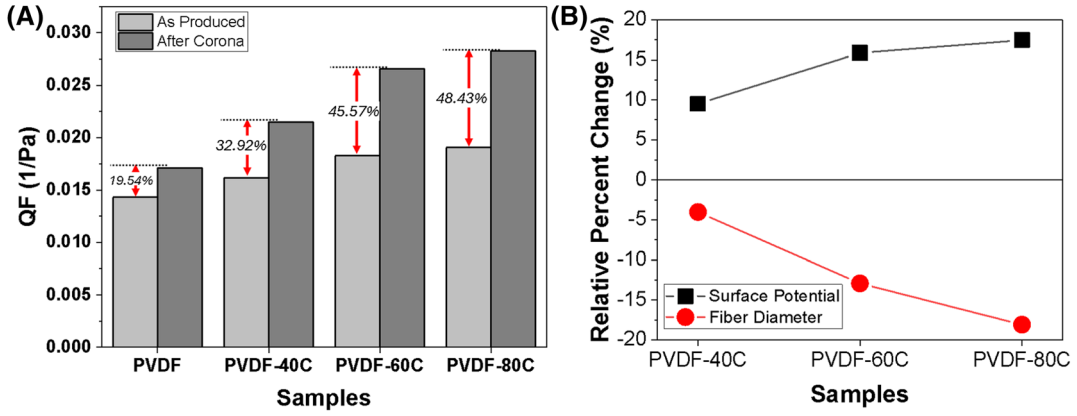

FIGURE 7 (A) QF values of the filter samples before and after corona discharge treatment and (B) relative percent changes in AFDs and surface potential corresponding to the improvement of the PVDF sample.

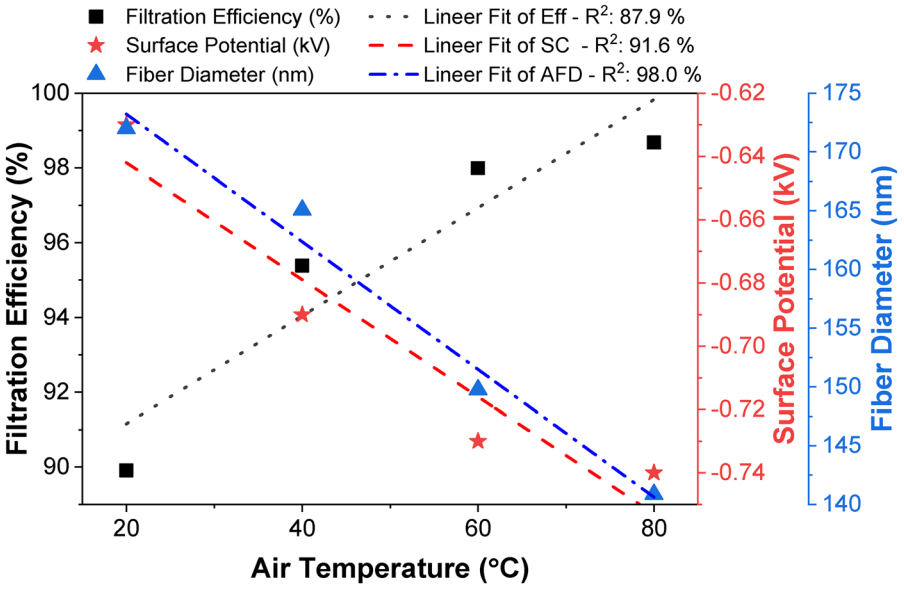

FIGURE 8 The relationship between temperature of blown air and filtration performance, surface potential, and the AFDs.

reveal a strong correlation between these parameters and the temperature of blown air, demonstrating that the properties of nanofibrous mats is significantly influenced by the temperature of the air used during the process. Specifically, correlations of 87.9% for filtration efficiency, 91.6% for surface potential, and 98% for AFD were observed. An increase in *blown* air temperature leads to a reduction in fiber diameter, accompanied by an improvement in both filtration efficiency and surface potential. The enhanced filtration performance can be attributed to the thinner fibers, which provide an increased surface area-to-volume ratio. Furthermore, the rise in surface potential can be explained by better alignment of polymer chains during the spinning process and the increased surface area offered by thinner fibers.

4 | CONCLUSION

This study underscores the pivotal role of compressed air temperature in shaping the morphology, porosity, crystallization, and filtration performance of PVDF nanofibers produced via the innovative electroblowing method. Elevated air temperatures were found to significantly enhance the homogeneity of fibers and defect-free structure of nanofibrous mats by reducing the AFDs as well as the occurrence of droplets and fiber bundles within the structure. Notably, while the AFD of PVDF samples produced *with un-heated blown air temperature* (*20°C*) was 172 nm, the PVDF-80C sample, fabricated at an air temperature of 80°C, exhibited a reduced fiber diameter of 140.9 nm. The thinner fibers and smaller pore sizes translated into superior filtration performance, as demonstrated by the PVDF-80C sample, which achieved an exceptional filtration efficiency of 98.68% against $PM_{0.3}$ aerosols at a flow rate of 95 L/min. Furthermore, higher air temperatures promoted β-phase formation, resulting in increased surface potential values, particularly after corona discharge process. These results highlight the critical influence of air temperature in optimizing the EB process and advancing the development of high-performance filtration materials.

DATA AVAILABILITY STATEMENT

Data available on request from the authors. The data that support the findings of this study are available from the corresponding author upon reasonable request.

ORCID

Ali Toptaş https://orcid.org/0000-0002-1176-0844

REFERENCES

1. Aguilar-Gomez S, Dwyer H, Zivin JG, Neidell M. This is air: the "nonhealth" effects of air pollution. *Annu Rev Resour Econ*. 2022;14:403-425. doi:10.1146/annurev-resource-111820-021816
2. Wang Q. Urbanization and Global Health: the role of air pollution. *Iran J Public Health*. 2018;47:1644-1652.
3. Ye C, Schröder P, Yang D, Chen M, Cui C, Zhuang L. Toward healthy and liveable cities: a new framework linking public health to urbanization. *Environ Res Lett*. 2022;17:064035. doi:10.1088/1748-9326/ac70eb
4. Wang S, Gao S, Li S, Feng K. Strategizing the relation between urbanization and air pollution: empirical evidence from global countries. *J Clean Prod*. 2020;243:118615. doi:10.1016/j.jclepro.2019.118615
5. Siddique HMA, Kiani AK. Industrial pollution and human health: evidence from middle-income countries. *Environ Sci Pollut Res*. 2020;27:12439-12448. doi:10.1007/s11356-020-07657-z
6. Maji S, Ahmed S, Kaur-Sidhu M, Mor S, Ravindra K. Health risks of major air pollutants, their drivers and mitigation strategies: a review. *Air Soil Water Res*. 2023;16:11786221231154659. doi:10.1177/11786221231154659
7. Lu F, Xu D, Cheng Y, et al. Systematic review and meta-analysis of the adverse health effects of ambient PM2.5 and

PM10 pollution in the Chinese population. *Environ Res*. 2015; 136:196-204. doi:10.1016/j.envres.2014.06.029
8. Feng J, Yang W. Effects of particulate air pollution on cardiovascular health: a population health risk assessment. *PLoS One*. 2012;7:e33385. doi:10.1371/journal.pone.0033385
9. Stanek LW, Brown JS. Air pollution: sources, regulation, and health effects. *Reference Module in Biomedical Sciences*. Elsevier; 2019. doi:10.1016/B978-0-12-801238-3.11384-4
10. Al-Harbi M, Alhajri I, Whalen JK. Characteristics and health risk assessment of heavy metal contamination from dust collected on household HVAC air filters. *Chemosphere*. 2021;277: 130276. doi:10.1016/j.chemosphere.2021.130276
11. Barhate RS, Ramakrishna S. Nanofibrous filtering media: filtration problems and solutions from tiny materials. *J Membr Sci*. 2007;296:1-8. doi:10.1016/j.memsci.2007.03.038
12. Vijayan VK, Paramesh H, Salvi SS, Dalal AAK. Enhancing indoor air quality: the air filter advantage. *Lung India*. 2015;32: 473-479. doi:10.4103/0970-2113.164174
13. Toptaş A, Çalışır M, Kılıç A. Optimization of electro-blown PVDF nanofibrous mats for air filter applications. *El-Cezeri*. 2024;11:199-206.
14. Kilic A, Selcuk S, Toptas A, Seyhan A. Chapter 10: nonelectro nanofiber spinning techniques. In: Kargari A, Matsuura T, Shirazi MMA, eds. *Electrospun and Nanofibrous Membranes*. Elsevier; 2023:267-293. doi:10.1016/B978-0-12-823032-9.00001-5
15. Alghoraibi I, Alomari S. Different methods for nanofiber design and fabrication. In: Barhoum A, Bechelany M, Makhlouf A, eds. *Handbook of Nanofibers*. Springer International Publishing; 2018:1-46. doi:10.1007/978-3-319-42789-8_11-2
16. Tibatan MA, Katana D, Yin CM. The emerging role of nanoscaffolds in chronic diabetic wound healing: a new horizon for advanced therapeutics. *J Biomater Sci Polym Ed*. 2024;1-32. doi: 10.1080/09205063.2024.2402148
17. Elnabawy E, Sun D, Shearer N, Shyha I. Electro-blown spinning: new insight into the effect of electric field and airflow hybridized forces on the production yield and characteristics of nanofiber membranes. *J Sci Adv Mater Dev*. 2023;8:100552. doi: 10.1016/j.jsamd.2023.100552
18. Zhou X, Li L, Li Z, Fan L, Kang W, Cheng B. The preparation of continuous CeO2/CuO/Al2O3 ultrafine fibers by electro-blowing spinning (EBS) and its photocatalytic activity. *J Mater Sci Mater Electron*. 2017;28:12580-12590. doi:10.1007/s10854-017-7082-4
19. Eticha A, Toptaş A, Akgül Y, Kiliç A. Electrically assisted solution blow spinning of PVDF/TPU nanofibrous mats for air filtration applications. *Turk J Chem*. 2023;47:47-53. doi:10.55730/1300-0527.3515
20. Gungor M, Toptas A, Calisir MD, Kilic A. Aerosol filtration performance of nanofibrous mats produced via electrically assisted industrial-scale solution blowing. *Polym Eng Sci*. 2021; 61:2557-2566. doi:10.1002/pen.25780
21. Angadjivand SA, Jones ME, Meyer DE. Method of charging electret filter media, US5496507A. 1996 https://patents.google.com/patent/US5496507A/en
22. Das D, Thakur R, Pradhan AK. Optimization of corona discharge process using box–Behnken design of experiments. *J Electrostat*. 2012;70:469-473. doi:10.1016/j.elstat.2012.07.005
23. Kilic A, Shim E, Pourdeyhimi B. Electrostatic capture efficiency enhancement of polypropylene electret filters with barium Titanate. *Aerosol Sci Tech*. 2015;49:666-673. doi:10.1080/02786826.2015.1061649
24. Castkova K, Kastyl J, Sobola D, et al. Structure–properties relationship of electrospun PVDF fibers. *Nanomaterials*. 2020;10: 1221. doi:10.3390/nano10061221
25. Tohluebaji N, Putson C, Muensit N. High electromechanical deformation based on structural Beta-phase content and electrostrictive properties of electrospun poly(vinylidene fluoride-hexafluoropropylene) nanofibers. *Polymers*. 2019;11:1817. doi: 10.3390/polym11111817
26. Gade H, Nikam S, Chase GG, Reneker DH. Effect of electrospinning conditions on β-phase and surface charge potential of PVDF fibers. *Polymer*. 2021;228:123902. doi:10.1016/j.polymer.2021.123902
27. Ghafari E, Jiang X, Lu N. Surface morphology and beta-phase formation of single polyvinylidene fluoride (PVDF) composite nanofibers. *Adv Compos Hybrid Mater*. 2018;1:332-340. doi:10.1007/s42114-017-0016-z
28. He Z, Rault F, Lewandowski M, Mohsenzadeh E, Salaün F. Electrospun PVDF nanofibers for piezoelectric applications: a review of the influence of electrospinning parameters on the β phase and crystallinity enhancement. *Polymers*. 2021;13:174. doi:10.3390/polym13020174
29. Zaarour B, Zhu L, Huang C, Jin X. Controlling the secondary surface morphology of electrospun PVDF nanofibers by regulating the solvent and relative humidity. *Nanoscale Res Lett*. 2018;13:285. doi:10.1186/s11671-018-2705-0
30. Cozza ES, Monticelli O, Marsano E, Cebe P. On the electrospinning of PVDF: influence of the experimental conditions on the nanofiber properties. *Polym Int*. 2013;62:41-48. doi:10.1002/pi.4314
31. Huang F, Wei Q, Wang J, Cai Y, Huang Y. Effect of temperature on structure, morphology and crystallinity of PVDF nanofibers via electrospinning. *E-Polymers*. 2008;8:152. doi:10.1515/epoly.2008.8.1.1758
32. Gregorio R Jr, Cestari M. Effect of crystallization temperature on the crystalline phase content and morphology of poly(vinylidene fluoride). *J Polym Sci B*. 1994;32:859-870. doi: 10.1002/polb.1994.090320509
33. Toptaş A, Çalışır MD, Kılıç A. Production of ultrafine PVDF nanofiber-/nanonet-based air filters via the Electroblowing technique by employing PEG as a pore-forming agent. *ACS Omega*. 2023;8:38557-38565. doi:10.1021/acsomega.3c05509
34. Ruan L, Yao X, Chang Y, Zhou L, Qin G, Zhang X. Properties and applications of the β phase poly(vinylidene fluoride). *Polymers (Basel)*. 2018;10:228. doi:10.3390/polym10030228
35. Cai X, Lei T, Sun D, Lin L. A critical analysis of the α, β and γ phases in poly(vinylidene fluoride) using FTIR. *RSC Adv*. 2017; 7:15382-15389. doi:10.1039/C7RA01267E
36. ISO 9237:1995. ISO. 2024 https://www.iso.org/standard/16869.html

How to cite this article: Toptaş A, Çalışır MD, Tibatan MA. Effect of blown air temperature on morphology, phase structure and filtration efficiency of PVDF nanofibrous mats produced via electro-blowing. *Polym Eng Sci*. 2025;65(4): 1868-1877. doi:10.1002/pen.27118